MMA, 83041-81-0; biacetyl, 431-03-8.

References and Notes

(1) Ishii, T.; Handa, T.; Matsunaga, S. *Macromolecules* **1978**, *11*, 40.
(2) Holden, D. A.; Guillet, J. E. *Macromolecules* **1980**, *13*, 289.
(3) Lindsell, W. E.; Robertson, F. C.; Soutar, I. *Eur. Polym. J.* **1981**, *17*, 203.
(4) Kano, K.; Takuma, K.; Ikeda, T.; Nakajima, D.; Tsutsui, Y.; Matsuo, T. *Photochem. Photobiol.* **1978**, *27*, 695.
(5) Ford, W. E.; Otvos, J. W.; Calvin, M. *Nature (London)* **1978**, *274*, 507.
(6) Turro, N. J.; Gratzel, M.; Braun, A. M. *Angew. Chem., Int. Ed. Engl.* **1980**, *19*, 675.
(7) Yanori, S. S.; Bovey, F. A.; Lumry, R. *Nature (London)* **1963**, *200*, 242.
(8) Vala, M. T., Jr.; Haebig, J.; Rice, S. A. *J. Chem. Phys.* **1965**, *43*, 886.
(9) David, C.; Piens, M.; Geuskens, G. *Eur. Polym. J.* **1972**, *8*, 1019.
(10) Aspler, J. S.; Guillet, J. E. *Macromolecules* **1979**, *12*, 1082.
(11) Fox, R. B.; Price, T. R.; Cozzens, R. F.; Echols, W. H. *Macromolecules* **1974**, *7*, 937.
(12) Holden, D. A.; Wang, P. Y.-K.; Guillet, J. E. *Macromolecules* **1980**, *13*, 295.
(13) Phillips, D.; Roberts, A. J.; Soutar, I. *Polymer* **1981**, *22*, 427.
(14) Phillips, D.; Roberts, A. J.; Soutar, I. *J. Polym. Sci., Polym. Phys. Ed.* **1980**, *18*, 2401. *Polymer* **1981**, *22*, 293.
(15) Nakahira, T.; Maruyama, T.; Iwabuchi, S.; Kojima, K. *Makromol. Chem.* **1979**, *180*, 1853.
(16) Nakahira, T.; Sakuma, T.; Iwabuchi, S.; Kojima, K. *Makromol. Chem., Rapid Commun.* **1980**, *1*, 437.
(17) Campaingene, E.; Heaton, B. G. *J. Org. Chem.* **1964**, *29*, 2372.
(18) Birks, J. B. "Photophysics of Aromatic Molecules"; Wiley-Interscience: New York, 1970; Chapters 7, 11.
(19) Abuin, E. A.; Lissi, E. A.; Gargallo, L.; Radic, D. *Eur. Polym. J.* **1980**, *16*, 793.
(20) David, C.; Piens, M.; Geuskens, G. *Eur. Polym. J.* **1976**, *12*, 621.
(21) Facile achievement of a planar geometry by the nearest-neighbor 2-naphthyl chromophores, compared with 1-naphthyl chromophores, has been confirmed by the emission characteristics of the dimeric model compounds (Chandross, E. A.; Dempster, C. J. *J. Am. Chem. Soc.* **1970**, *92*, 3586) as well as by the polymer molecular models (Sommersall, C.; Guillet, J. E. *Macromolecules* **1973**, *6*, 218).
(22) Noyes, R. M. *Prog. React. Kinet.* **1961**, *1*, 131.
(23) Birks, J. B.; Leite, M. S. S. C. P. *J. Phys. B* **1970**, *3*, 417.
(24) Sandros, K. *Acta Chem. Scand.* **1969**, *23*, 2815.
(25) Tyrell, H. J. V. "Diffusion and Heat Flow in Liquids"; Butterworths: London, 1961.
(26) n^{21}_D(THF) = 1.40762 and n^{21}_D(2-MeTHF) = 1.40595 ("Encyclopaedia Chimica"; Kyoritsu Shuppan: Tokyo, 1962).
(27) North, A. M.; Treadaway, M. F. *Eur. Polym. J.* **1973**, *9*, 609.
(28) The k_{DM} values are 1 order smaller than that obtained with poly(1-naphthyl methacrylate), 3.9×10^8 s^{-1},[10] which is comparable to the rate of rotational relaxation of the 2-naphthyl methacrylate residue in poly(methyl methacrylate-*co*-2-naphthyl methacrylate), 6×10^8 s^{-1} (Kettle, G. J.; Soutar, I. *Eur. Polym. J.* **1978**, *14*, 895). Since more bonds are involved in the present polymers, the rotational relaxation must proceed even faster; however, due to the larger chromophore separation, rotational relaxation does not appear to lead directly to excimer formation in these polymers.
(29) Birks, J. B.; Christophorou, L. G. *Proc. R. Soc. London, Ser. A* **1964**, *277*, 571.
(30) The fraction of preformed excimer pairs has been estimated to be as low as 10^{-3}–10^{-2} even in polymers with chromophores directly attached to the polymer main chain, e.g., poly(2-vinylnaphthalene)[33] and poly(*N*-vinylcarbazole) (Klöpffer, W. *J. Chem. Phys.* **1969**, *50*, 2337). We may reasonably expect that the corresponding fractions in these methacrylate polymers are considerably smaller than these values.
(31) Webber, S. E.; Avots-Avotins, P. E.; Deumie, M. *Macromolecules* **1981**, *14*, 104.
(32) The films of the copolymers containing 3–4 mol % of the naphthalene residue exhibited, as expected, only monomer emission, regardless of the pendant group structure.
(33) Frank, C. W.; Harrah, L. A. *J. Chem. Phys.* **1974**, *61*, 1526.
(34) Frank, C. W.; Gashgari, M. A. *Macromolecules* **1979**, *12*, 165.
(35) Irie, M.; Kamijo, T.; Aikawa, M.; Takemura, T.; Hayashi, K.; Baba, H. *J. Phys. Chem.* **1977**, *81*, 1571.
(36) Johnson, G. E. *J. Chem. Phys.* **1975**, *62*, 4697.

Properties of Racemic and Optically Active Poly(α-methyl-α-ethyl-β-propiolactones)

Daniel Grenier and Robert E. Prud'homme*

Groupe de Recherche sur les Macromolécules, Chemistry Department, Laval University, Québec, Canada G1K 7P4. *Received March 12, 1982*

ABSTRACT: Optically active and racemic poly(α-methyl-α-ethyl-β-propiolactones) (PMEPL) were studied by calorimetry (crystallization and fusion), polarized microscopy, small-angle light scattering, X-ray diffraction, and static and dynamic mechanical methods. Optically active PMEPL's have higher equilibrium melting points, enthalpies of fusion, and crystallization rates than the racemic PMEPL's. They have lower solubilities, different crystal structures, but similar T_g's. PMEPL's of intermediate optical purities were also studied. The observed results are discussed in terms of the stereoregularity of PMEPL chains. They are compared to the properties of other poly(α,α-disubstituted-β-propiolactones).

Introduction

Racemic monomers may lead to optically active polymers via a stereoselective polymerization. For example, optically active polyoxiranes and polythiiranes were prepared in this fashion.[1-4] However, this method leads to poly(α-methyl-α-*n*-propyl-β-propiolactones) (PMPPL) of low optical purities[5,6] and the physical properties of the racemic and optically active PMPPL's were shown to be very similar.[7]

High optical purity polylactones, similar to the high optical purity polyamides prepared by Schmidt[8] from β-lactams containing one or two asymmetric centers, must then be prepared from lactone enantiomers. Schmidt showed that the optically active poly(β-amides) have higher melting points and lower solubilities than the corresponding racemic polymers. Similarly, D'Hondt and Lenz[9] and Carrière and Eisenbach[10] prepared poly(α-phenyl-α-ethyl-β-propiolactones) (PPEPL) having optical purities of 80 and 95%, respectively. They showed that optically active PPEPL's have a melting point of about 130 °C higher than the racemic PPEPL's.

More recently, we have prepared poly(α-methyl-α-ethyl-β-propiolactones)[11] (PMEPL) having optical purities of 99%. We have shown that the high optical purity PMEPL's have a higher melting point, T_f, and a higher enthalpy of fusion, ΔH_f, than the racemic one, in agreement with the previous examples. However, the increase in T_f and ΔH_f is not linear: T_f and ΔH_f remain constant

0024-9297/83/2216-0302$01.50/0

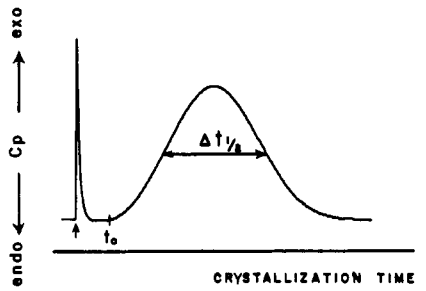

Figure 1. Typical DSC crystallization exotherm. The arrow indicates when the sample reaches the crystallization temperature. This is followed by a temporary thermal imbalance. t_0 is the time when the crystallization begins.

up to optical purities of 55% and then they increase rapidly.

It is the purpose of the present paper to investigate the thermal, mechanical, optical, and crystalline properties of PMEPL's of different degrees of optical purity. These properties will be compared to those of other disubstituted polylactones.

Experimental Section

PMEPL's were polymerized from α-methyl-α-ethyl-β-propiolactone (MEPL). A potassium acetate/dicyclohexyl-18-crown-6 complex was used as anionic initiator.[11] All polymerizations were carried out in tetrahydrofuran at 55 °C. Using a racemic MEPL, the *S*(−) enantiomer, and the *R*(+) enantiomer, we prepared several PMEPL's: a racemic polymer (PMEPL-RAC), three *S*(−)-enriched polyesters whose optical purities equal 27, 55, and 74% (PMEPL-*S*(−)-27, PMEPL-*S*(−)-55, and PMEPL-*S*(−)-74), and two high optical purity homopolymers (PMEPL-*S*(−)-99 and PMEPL-*R*(+)-97). The initial *S*(−) and *R*(+) enantiomers had optical purities of 99 and 97%, respectively. The molecular weights of all polymers are close to 50 000.

The crystallization and melting experiments were conducted on a Perkin-Elmer DSC-1B differential scanning calorimeter calibrated with pure indium and gallium. Heating rates of 20 °C/min were used in all cases; we have verified that the melting temperatures and enthalpies of fusion were identical for smaller heating rates.

The polymer samples were melted, kept at about 30 °C above their melting point for 5 min, and brought rapidly to the crystallization temperature, where the crystallization exotherms were recorded (Figure 1). It can be shown[12] that the width at half-height, $\Delta t_{1/2}$, of the exotherm is directly proportional to the time of half-crystallization, $t_{1/2}$. The proportionality constant between $\Delta t_{1/2}$ and $t_{1/2}$ is only a function of the nucleation mode and of the dimensionality of the crystal growth.

For mechanical property measurements, polymer films were prepared by solvent casting from a chloroform solution on a mercury bath at room temperature. Stress–strain curves were obtained on an Instron tester, table model 1130. Dynamic mechanical properties measurements were made with a Rheovibron DDV-II apparatus at 110 Hz.

X-ray measurements were conducted on an X-ray apparatus consisting of a Philips generator equipped with a Warhus-Statton camera. A Cu Kα target was used and the incident beam was nickel filtered. The camera was calibrated with NaCl crystals.

Microscopy measurements were made with a Zeiss polarizing microscope. Small-angle light scattering (SALS) patterns were recorded with an apparatus consisting of a He–Ne laser, a polarizer, an analyzer, a microscope stage, a shutter, and a Polaroid camera.[13] So-called H_v SALS patterns were obtained, the polarizer being vertical and the analyzer horizontal. For SALS, samples were melted on a Mettler hot stage and slowly cooled to room temperature at a cooling rate of 0.2 °C/min. Finally, glass transition temperature measurements were also conducted on the DSC-1B apparatus.

Results

Calorimetry. Figure 2 shows the PMEPL's melting endotherms for samples crystallized at a supercooling of 60 °C. The racemic polymer shows two melting peaks and the surface area of its low-temperature peak (peak 2) increases regularly with the crystallization temperature, T_c, whereas the surface area of its high-temperature peak (peak 1) decreases, as shown in Figure 3.

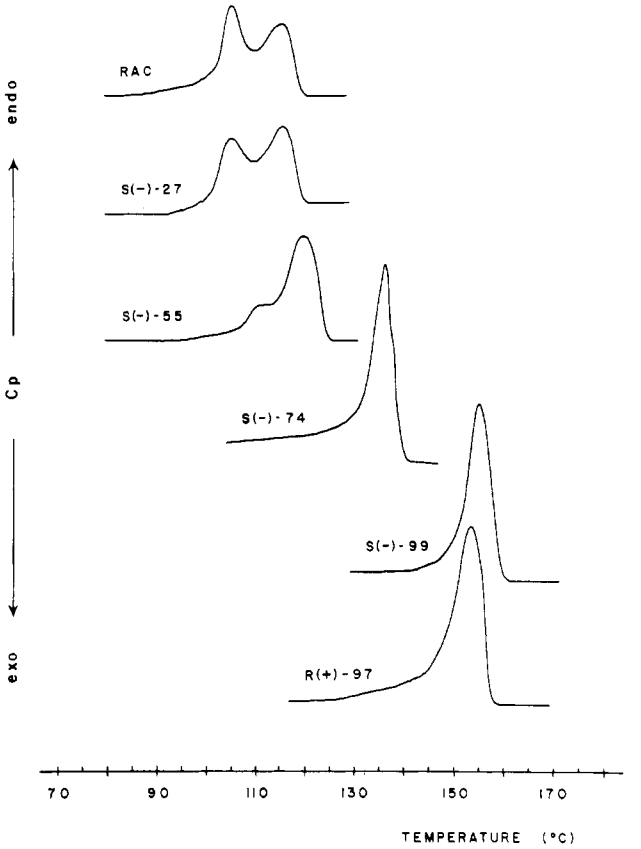

Figure 2. PMEPL melting endotherms at a supercooling of 60 °C.

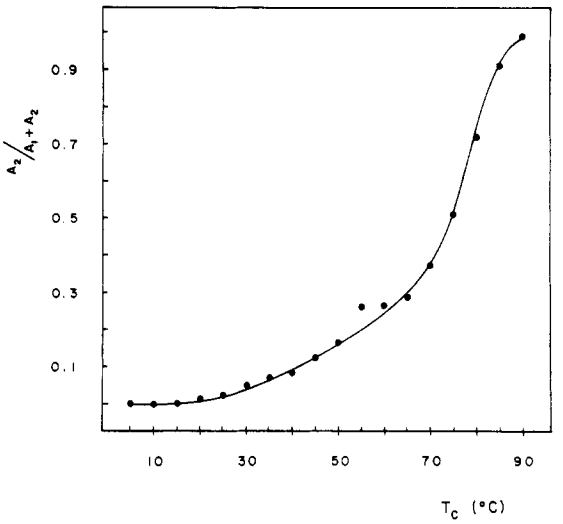

Figure 3. Fractional surface area of peak 2 as a function of the crystallization temperature T_c. A_2 is the surface area of peak 2 and A_1 that of peak 1.

The observation of a melting endotherm with two maxima is a common feature of semicrystalline polymers. It has been reported for isotactic polystyrene,[14,15] for poly(ethylene terephthalate),[16,17] for nylon 6,6,[18,19] and for several polylactones: poly(pivalolactone),[20,21] poly(β-propiolactone),[22] poly(α,α-diethyl-β-propiolactone),[23] and poly(α-methyl-α-*n*-propyl-β-propiolactone),[7] to mention just a few examples. These two maxima are sometimes

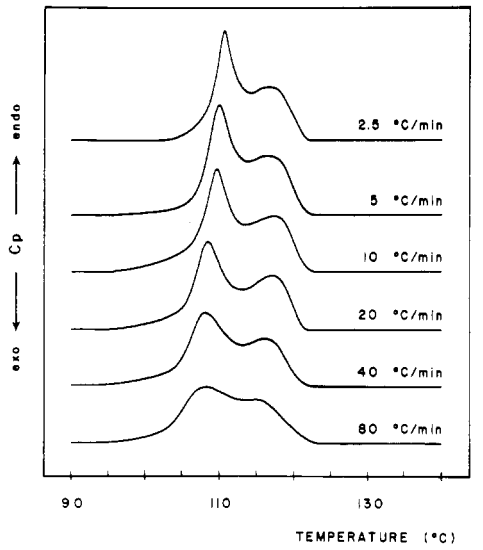

Figure 4. PMEPL-RAC melting endotherms at different heating rates.

related to the presence of two different crystal structures. More often, they are related to the presence of two different morphological structures. For PMEPL-RAC, the same X-ray diffraction patterns were found for samples crystallized at 30 and 85 °C. In the first case, peak 1 is the most important one and in the latter case, peak 2 has a greater surface area than peak 1 (Figure 3). The same crystal structure is then found for peaks 1 and 2 and their origin must be morphological.

It has also been proposed that melting endotherms with two maxima result from the melting of peak 2 followed by the recrystallization of the polymer and its remelting at a higher temperature (peak 1) during the DSC run; peak 1 then results from the thickening of the polymer lamellae. When this process occurs, the relative surface areas of peaks 1 and 2 depend upon the heating rate, peak 1 surface area decreasing with increasing heating rates.[7,20,23-25] This explanation does not hold for PMEPL-RAC since the relative surface areas of peaks 1 and 2 do not change significantly with heating rates, at a given crystallization temperature, as is shown in Figure 4.

Figure 2 also shows that PMEPL-*S*(−)-99 exhibits a narrow melting endotherm. Measurements made at different T_c's indicate that this peak is composed of two different peaks that are poorly resolved; peak 2 gets closer to peak 1 with increasing T_c since the width at half-height of the endotherm goes gradually from 6.6 to 5.5 °C when T_c increases from 105 to 140 °C. The resolution of these two peaks could not be made at any T_c and a single melting point T_f was determined at the end of the endotherm whereas for PMEPL-RAC, peaks 1 and 2 were resolved and two T_f's were recorded at the end of each peak.

Samples PMEPL-*S*(−)-27 and PMEPL-*R*(+)-97 have a melting behavior identical with that of samples PMEPL-RAC and PMEPL-*S*(−)-99, respectively.

Samples PMEPL-*S*(−)-55 and PMEPL-*S*(−)-74 have a melting behavior intermediate between that of samples PMEPL-RAC and PMEPL-*S*(−)-99. The melting endotherms shown in Figure 2, the equilibrium melting points $T_f°$, and the enthalpies of fusion ΔH_f given in Table I, however, indicate that PMEPL-*S*(−)-55 is more similar to PMEPL-RAC while PMEPL-*S*(−)-74 is more similar to PMEPL-*S*(−)-99.

Figure 5 shows a plot of T_f vs. T_c for several PMEPL's. Two T_f's are reported for PMEPL-RAC and only one for the others. As shown in Table I, the resolution of peaks

Table I
PMEPL Glass Transition Temperature, T_g, Enthalpy of Fusion, ΔH_f, and Equilibrium Melting Temperature of Peaks 1 ($T_{f(1)}°$) and 2 ($T_{f(2)}°$)

polymer	T_g/ °C	ΔH_f/ (J/g)	$T_{f(1)}°$/ °C	$T_{f(2)}°$/ °C
PMEPL-RAC	−17	27	121	134
PMEPL-*S*(−)-27	−17	27	120	134
PMEPL-*S*(−)-55	−16	38	125	134
PMEPL-*S*(−)-74	−15	59	145	
PMEPL-*S*(−)-99	−15	59	164	
PMEPL-*R*(+)-97	−15	60	163	

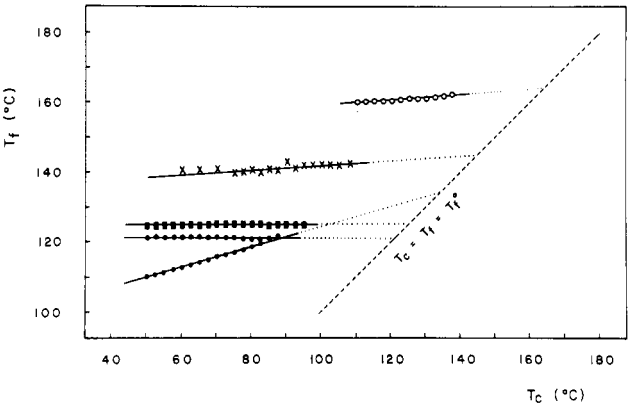

Figure 5. Melting temperature, T_f, vs. crystallization temperature, T_c, for PMEPL-RAC (●), PMEPL-*S*(−)-55 (■), PMEPL-*S*(−)-74 (×), and PMEPL-*S*(−)-99 (○).

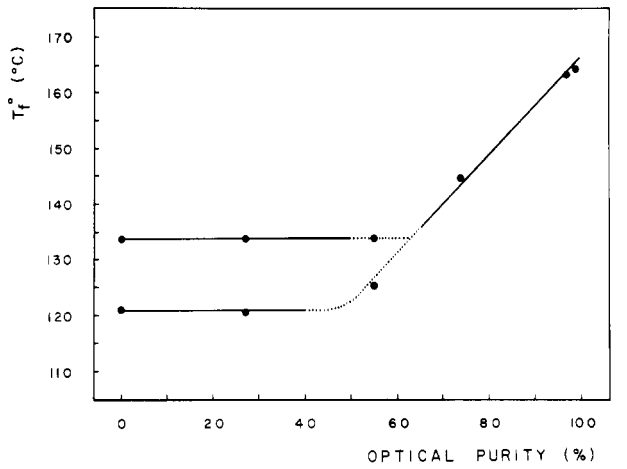

Figure 6. Equilibrium melting point, $T_f°$, vs. optical purity of PMEPL's.

1 and 2 could not be made for the higher optical purity samples. [The second T_f of PMEPL-*S*(−)-55 is not drawn on Figure 5 for clarity reasons.] It is seen that the T_f of peak 1 does not depend much upon T_c whereas the T_f of peak 2 changes rapidly with T_c. It is also seen that peak 2 gets closer to peak 1 as T_c increases. For both peaks, T_f can be extrapolated to the point where $T_f = T_c$ according to the Hoffman–Weeks method.[26] This points defines $T_f°$. Values of $T_f°$ obtained in this manner are given in Table I.

Figure 6 shows that both $T_f°$'s remain the same up to optical purities of 50%. For larger optical purities, both values get very close and they increase regularly up to a value of 164 °C.

ΔH_f values were recorded for all PMEPL's at several T_c's. As mentioned before, ΔH_f of peak 2 increases and ΔH_f of peak 1 decreases with increasing T_c. However, the total value of ΔH_f remains constant for each PMEPL. This result is similar to that observed previously with poly-

Table II
Crystallization Kinetics Parameters of PMEPL's, Poly(pivalolactone) (PPL), Poly(α-methyl-α-n-propyl-β-propiolactone) (PMPPL), Poly(α,α-diethyl-β-propiolactone) (PDEPL), Poly(ethylene sebacate) (PES), and Poly(ethylene adipate) (PEA)

polymer	peak (regime)	A/nm²	$\sigma \times 10^{-7}$/ (J/cm²)	G_0/s⁻¹	U^*/ (kJ/mol)	K_g/K	$\sigma_e \times 10^{-7}$/ (J/cm²)	q/ (kJ/mol)
PMEPL-RAC	1 (II)	0.502	11	7.64×10^5	8.6	324	41	18
	2 (I)	0.502	11	9.00×10^8	10.8	626	39	17
PMEPL-S(−)-27	1 (II)	0.496	a	2.33×10^6	9.4	334	42	19
	2 (I)	0.496	a	2.70×10^9	11.6	645	41	18
PMEPL-S(−)-55	1 (II)	a	a	8.14×10^3	4.3	337	42	19
	2 (I)	a	a	7.92×10^7	7.5	674	42	19
PMEPL-S(−)-74	1 (II)	0.519	b	4.73×10^6	11.0	361	44	14
PMEPL-S(−)-99	1 (II)	0.522	20	6.83×10^{10}	23.5	381	46	16
PMEPL-R(+)-97	1 (II)	0.528	b	1.63×10^7	13.0	379	45	15
PPL[42]		0.447	18				43	18
PMPPL[43]	1 (I)	0.568	17		17.2	624	35	12
PDEPL[23]	2 (I)		12	3.16×10^{10}	17.2	642	40	17
PES[37]	(II)	0.365	9		17.2	95	41	14
PEA[37]	(II)	0.363	9		17.2	106	45	16

[a] Used the value of PMEPL-RAC. [b] Used the value of PMEPL-S(−)-99.

(α,α-diethyl-β-propiolactone).[23] For PMEPL, the total value of ΔH_f follows the same trend as $T_f°$ as a function of optical purity (Table I).

It is well-known that a diluent added to a semicrystalline polymer will lead to a decrease in melting point which is predicted as follows:[27]

$$\frac{1}{T_f} - \frac{1}{T_f'} = \frac{R}{\Delta H°}\frac{v}{v_1}\left[\phi_1 - \frac{Bv_1}{RT_f}\phi_1^2\right] \quad (1)$$

where T_f is the melting temperature of the polymer containing a diluent, T_f' is the melting temperature of the pure polymer, R is the gas constant, $\Delta H°$ is the enthalpy of fusion of the fully crystallized polymer, v and v_1 are the molar volumes of the polymer repeat unit and of the diluent, ϕ_1 is the diluent volume fraction, and B is the polymer–diluent interaction parameter. As shown in Figure 7 for PMEPL/dibutyl phthalate mixtures, a plot of $(1/T_f - 1/T_f')/\phi_1$ vs. ϕ_1/T_f leads to a straight line whose intercept equals $(R/\Delta H°)(v/v_1)$. The data of Figure 7 lead to $\Delta H°$'s equal to 9.6 and 17.5 kJ/mol for PMEPL-RAC and PMEPL-S(−)-99, respectively. Using these values and the ΔH's given in Table I, one computes a degree of crystallinity of 31% for the former sample and a degree of crystallinity of 39% for the latter.

Polymer crystal growth rates, G, obey the Turnbull–Fisher equation:[28]

$$G = G_0 \exp[\Delta F^*/kT_c] \exp[\Delta\phi^*/kT_c] \quad (2)$$

where ΔF^* is the transport free activation energy at the liquid–solid interface, $\Delta\phi^*$ is the free energy of formation of a crystal of critical size, k is the Boltzmann constant, and G_0 is a constant. Following Hoffman,[29] Suzuki and Kovacs[30] have recently tested several expressions of ΔF^* and $\Delta\phi^*$. They finally proposed the equation

$$G = G_0 \exp\left[\frac{U^*}{R(T_c - T_\infty)}\right] \exp\left[-K_g\frac{T_f°(T_f° + T_c)}{2T_c^2(T_f° - T_c)}\right] \quad (3)$$

where U^* is a parameter related to the viscosity of the melt,[31] K_g is a constant that will be discussed below, and T_∞ is the temperature where all molecular motion associated with viscous flow ceases. T_∞ can be set equal to $(T_g - 30)$,[30,32-36] T_g being the glass transition temperature.

We have observed the heterogeneous nucleation of all PMEPL samples[12] and have assumed that the concentration of nuclei is constant as a function of T_c, not too close to T_m.[37,59] Then the width at half-height, $\Delta t_{1/2}$, of the crystallization exotherms can be related to the growth rate:[12,37]

$$G \simeq 1/\Delta t_{1/2} \quad (4)$$

The experimental values of $\Delta t_{1/2}$, $(\Delta t_{1/2})_{exptl}$, can then be compared with the theoretical values, $(\Delta t_{1/2})_{calcd}$, calculated with eq 3 and 4. This calculation was made for PMEPL's by an iterative method where the parameters U^*, K_g, and G_0 were chosen such as to give the smallest standard deviation, ϕ, for each curve, where

$$\phi = \left[\frac{1}{n}\sum_{i=1}^{n}((1/\Delta t_{1/2})_{calcd} - (1/\Delta t_{1/2})_{exptl})_i^2\right]^{0.5} \quad (5)$$

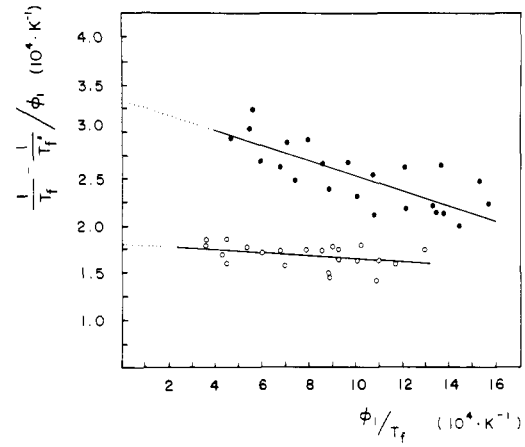

Figure 7. PMEPL/dibutyl phthalate melting point data according to eq 1. The full circle data were obtained for PMEPL-S(−)-99 and the empty circle data for PMEPL-RAC.

Figure 8 shows the experimental values of $1/\Delta t_{1/2}$ as a function of the reduced crystallization temperature $(T_c - T_g)/(T_f° - T_g)$, on which are superposed the calculated curves. The calculations were made by using the U^*, K_g, and G_0 parameters listed in Table II. For PMEPL-RAC, PMEPL-S(−)-27, and PMEPL-S(−)-55, two values of K_g were calculated from the two $T_f°$'s listed in Table I. From Figure 8, it is seen that the growth rate increases significantly with optical purity and that each series of data can be represented satisfactorily by the theory.

Polymer crystal growth obeys one of the two following crystallization regimes:[38] under regime I, each surface nucleus leads to the rapid addition of a polymer layer on the surface of the crystal before a new nucleus can occur; under regime II, a large number of surface nuclei form on

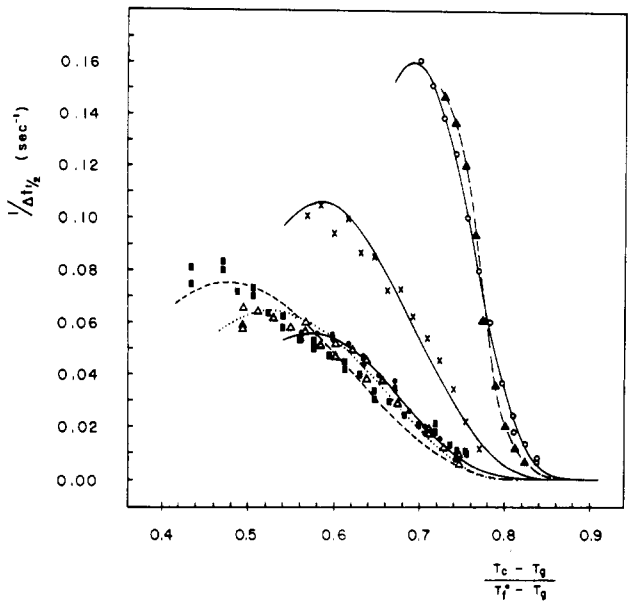

Figure 8. Crystallization rate, $(\Delta t_{1/2})^{-1}$, vs. the reduced crystallization temperature for PMEPL-RAC (●), PMEPL-*S*(−)-27 (△), PMEPL-*S*(−)-55 (■), PMEPL-*S*(−)-74 (×), PMEPL-*S*(−)-99 (○), and PMEPL-*S*(−)-97 (▲). The curves were drawn according to eq 3 and 4.

the crystal and their lateral growth is slow. Lauritzen[39] has shown that it is possible to distinguish between regimes I and II by making a comparison between the crystalline lamellae width, L, calculated in each case since

regime I: $$L \leq 2a'(10^{-5} \exp[K_g/(T_c(T_f^\circ - T_c))])^{0.5} \quad (6a)$$

regime II: $$L \geq 2a'(10^{-3} \exp[2K_g/(T_c(T_f^\circ - T_c))])^{0.5} \quad (6b)$$

where a' is the width of the polymer molecule (see the Crystal Structure Analysis section, from which it can be shown that $a' = a/2$ for PMEPL's). For the experimental values of K_g, T_c, and T_f°, two values of L are then calculated and normally one of these two values is unrealistic, which allows the rejection of the corresponding regime (L is expected to lie somewhere in the range 50–1000 nm]. Using this method, it was possible to conclude that PMEPL crystallization obeys regime II when $T_{f(1)}^\circ$ is used; it obeys regime II when $T_{f(2)}^\circ$ is used (Table II).

The lateral surface interfacial free energy, σ, the fold surface interfacial free energy, σ_e, and the work required to fold a chain, q, can be calculated from the following relations:[29,40,41]

$$\sigma = 0.11a'\Delta H^\circ \quad (7a)$$

$$\sigma_e = k/(0.11yA)K_g \quad (7b)$$

$$q = 2A(\sigma_e - \sigma) \quad (7c)$$

where A is the chain cross-sectional area ($A = (ab \sin \gamma)/2$; see the Crystal Structure Analysis section) and y is a constant equal to 4 in regime I and equal to 2 in regime II.

In Table II, PMEPL σ_e and q values are reported. It is remarkable that all of them are, within experimental error, constant. They are also identical with the values reported in the literature for several other polyesters. The constancy of these values may appear surprising but it must be remembered that q is a parameter that is related to the structure of the amorphous chain and not of the crystallized chain. Constant values of q indicate that the folding of a PMEPL chain does not depend upon its

Table III
PMEPL Spherulite Radii Measured by Small-Angle Light Scattering

polymer	radius/ μm	polymer	radius/ μm
PMEPL-RAC	30	PMEPL-*S*(−)-74	7.5
PMEPL-*S*(−)-27	27	PMEPL-*S*(−)-99	4.2
PMEPL-*S*(−)-55	9.8	PMEPL-*R*(+)-97	4.6

stereoregularity as measured by optical purity and that the folding of poly(α,α-disubstituted-β-propiolactones) and of poly(β-monosubstituted-β-propiolactones) does not depend upon the size of the substituents on the chain. Small fluctuations observed in Table II, from 41×10^{-7} to 45×10^{-7} J/cm^2 for σ_e and from 15 to 18 kJ/mol for q, are not significant.

Morphology. Polarized microscopy and small-angle light scattering (SALS) techniques were used to study the morphology of PMEPL's.

As shown in Figure 9, all samples give rise to a spherulitic morphology. The spherulites are, however, very large for PMEPL-RAC (and PMEPL-*S*(−)-27), smaller for PMEPL-*S*(−)-55, and very small, of the order of a few microns, for the other samples. The spherulitic structure is not well resolved by microscopy in the latter case, but the four-leaf-clover pattern observed by SALS leaves no doubt. On the other hand, large spherulites are seen by microscopy for the former samples but the corresponding SALS four-leaf-clover pattern is not well defined because the number of spherulites under illumination is small and because interspherulitic interference occurs, leading to a highly speckled pattern.[44]

From SALS, the average radius of the spherulites, R, can be determined by[45]

$$R = 4.1\lambda/4\pi \sin(\theta/2) \quad (8)$$

where λ is the wavelength of the scattered light in the scattering medium and θ is the scattering angle where the maximum in intensity of the clover-leaf pattern is found, after correction for the air–sample interface. PMEPL's spherulite sizes were determined and are reported in Table III. Radii of about 30 μm were found for low optical purity samples. These radii decrease regularly with increasing optical purities down to about 4 μm for PMEPL-*S*(−)-99.

Mechanical Properties. Stress–strain curves of PMEPL's were recorded. Low optical purity samples are highly deformable and can be stretched up to elongations of several tenth percent as reported before.[46] They show a yield point, a necking phenomenon, and a ductile fracture. High optical purity samples show a fragile fracture at an elongation of about 4% before any yield point. In all samples, the Young's modulus is about 310 MPa. Schmidt[8] also observed similar Young's moduli for optically active and racemic poly(β-butyrolactams).

An α–β transition has been reported before for racemic PMEPL,[46] where form α has a 2_1 helical chain conformation and form β a planar-zigzag chain conformation. Low optical purity PMEPL's show this transition but high optical purity PMEPL's do not since the samples break before the yield point from which the transition starts.

Dynamic mechanical properties are reported in Figure 10 for PMEPL-RAC and PMEPL-*S*(−)-99. In both cases, a single huge peak is seen but that of the latter sample is broader than that of the former. The maximum of this peak is found at 17 ± 3 and 25 ± 3 °C for PMEPL-RAC and PMEPL-*S*(−)-99, respectively. If this maximum temperature is associated to T_g, it is concluded that the T_g's of racemic and optically active PMEPL's are close, in agreement with the DSC T_g's (Table I). The dynamic

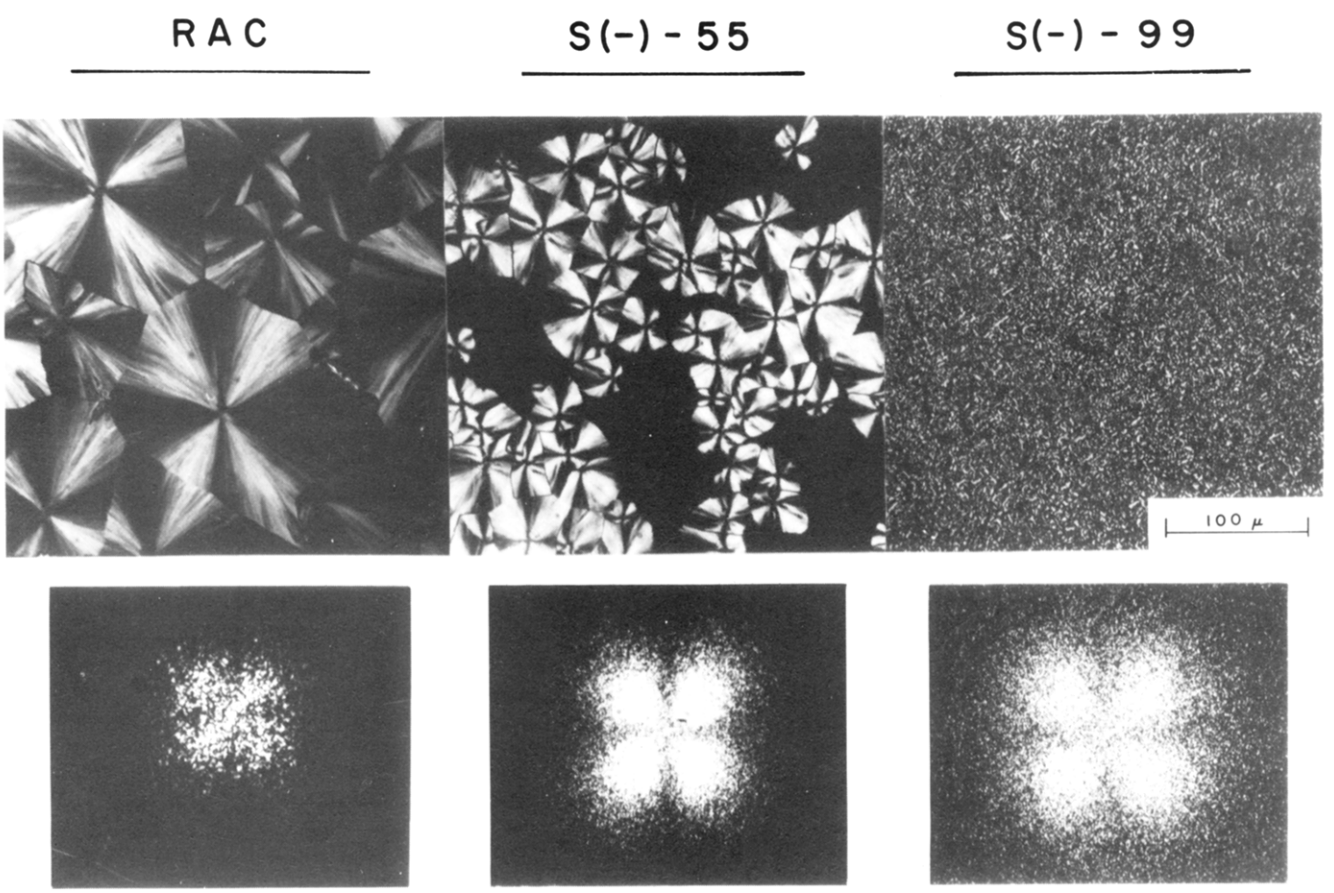

Figure 9. Photomicrographs (top) and H_v small-angle light scattering patterns (bottom) for PMEPL-RAC, PMEPL-*S*(−)-55, and PMEPL-*S*(−)-99 crystallized by slowly cooling at a rate of 0.2 °C/min from the melt. (SALS patterns were not taken at the same sample–film distance.)

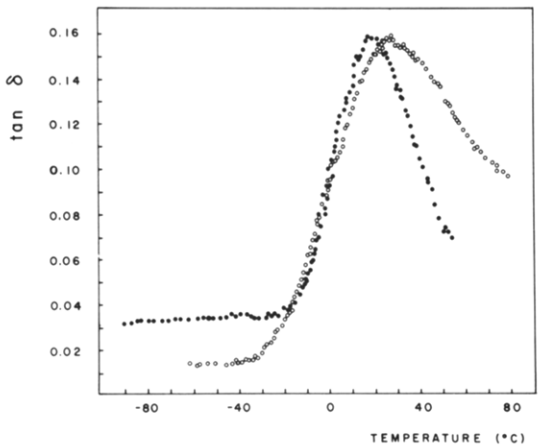

Figure 10. PMEPL-RAC (●) and PMEPL-*S*(−)-99 (○) values of tan δ as a function of temperature at 110 Hz.

mechanical T_g's are, however, much higher than the DSC T_g's because the former measurements were made at a high frequency. The PMEPL-RAC tan δ curve shown in Figure 10 is similar to that reported before.[46]

Crystal Structure Analysis. Highly oriented optically active PMEPL films and fibers could not be obtained. Highly oriented racemic PMEPL films could be obtained but, as mentioned above, an α–β transition occurs upon orientation and the oriented polymer corresponds to form β. X-ray fiber patterns of form α could not be obtained in any case. The PMEPL crystal structure analysis was then carried out on unoriented samples.

The X-ray diffraction patterns of samples PMEPL-RAC and PMEPL-*S*(−)-99 are shown in Figure 11. Important differences are seen between the peak positions and intensities of the two patterns, suggesting different unit cell parameters.

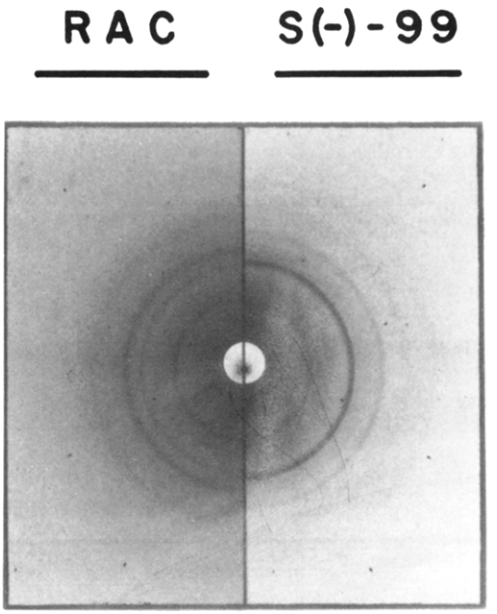

Figure 11. X-ray diffraction patterns of PMEPL-RAC and PMEPL-*S*(−)-99.

It is, however, noticed that there are similarities between these two patterns and that of poly(pivalolactone) (PPL).[47,48] For example, the peak with the highest intensity, corresponding to the (100) plane of PPL, is found at interplanar spacings of 0.764 nm for PPL, of 0.850 nm for PMEPL-RAC, and of 0.907 nm for PMEPL-*S*(−)-99. The peak with the second highest intensity is observed at

interplanar spacings of 0.571, 0.586, and 0.565 nm for PPL, PMEPL-RAC, and PMEPL-*S*(−)-99, respectively. Similarly, a third peak of high intensity is found at interplanar spacings of 0.492, 0.510, and 0.495 nm for the same three polymers. It is possible to proceed in the same manner for each peak of the PMEPL patterns and to find a corresponding peak on the PPL pattern.

In view of this similarity between PMEPL and PPL patterns, we have assumed a similar crystal structure in both cases. The PPL Miller indices have been associated to the corresponding PMEPL peaks. Assuming a monoclinic unit cell having dimensions a, b, and c and an angle γ, we calculated interplanar spacings (d_{calcd}) and compared them with the experimental values (d_{exptl}):

$$\frac{1}{d_{calcd}^2} = \frac{h^2}{a^2 \sin^2 \gamma} + \frac{k^2}{b^2 \sin^2 \gamma} + \frac{l^2}{c^2} - \frac{2hk}{ab \sin^2 \gamma} \cos (180 - \gamma) \quad (9)$$

Values of a, b, c, and γ were changed by an iteration procedure and the values leading to the smallest standard deviation, ϕ, between d_{calcd} and d_{exptl} were retained. As shown in Table IV, a satisfactory agreement between d_{calcd} and d_{exptl} is found by this method, which was applied to all PMEPL's except PMEPL-*S*(−)-55, for which a satisfactory agreement could not be found. In that particular case, a comparison of the X-ray diffraction pattern with those of PMEPL-RAC and PMEPL-*S*(−)-99 indicates that it contains all peaks of the former sample and some peaks of the latter one. This result suggests that this polymer contains a small amount of long isotactic blocks of *S* configuration that can crystallize like PMEPL-*S*(−)-99. The remaining segments of the polymer are forming short isotactic blocks that crystallize like PMEPL-RAC.

Table V lists the PMEPL unit cell dimensions obtained by the above procedure. This iterative method was also applied to PPL and PMPPL and it leads to the literature values: the unit cell dimensions reported in Table V for these two polymers were calculated in this manner. Attempts were initially made to force $\gamma = 90°$ (orthorhombic unit cell). These attempts led to exceedingly large ϕ. The periodicity of all PMEPL's is found close to 0.6 nm, suggesting a 2_1 helical conformation for these polymers, as found for PPL, PMPPL, and PβBL.

From unit cell dimensions, the PMEPL crystal density was calculated assuming four polymer repeat units per unit cell. The densities calculated are slightly larger than those measured for the semicrystalline polymers. Some amorphous densities are given in Table V. These were calculated from the crystal density, the polymer density, and the degree of crystallinity determined from ΔH_f (Table I) and $\Delta H°$.

Table V indicates that PMEPL-RAC and PMEPL-*S*-(−)-27 have, within experimental error, the same unit cell dimensions. PMEPL-*S*(−)-99 and PMEPL-*R*(+)-97 have also, within experimental error, the same unit cell dimensions. However, the dimensions of the racemic polymer unit cell are slightly different from those of the optically active polymers. PMEPL-*S*(−)-74 has unit cell dimensions similar to those of the optically active polymers. Its isotactic content is high but not as much as for polymers of higher optical purity. It crystallizes in the same crystal structure as the latter but its smaller isotactic content leads to smaller $T_f°$ values.

Discussion

Polylactones, having the general formula $-[CHR_3CR_1R_2COO]-_n$, are usually found in a helical 2_1

Table IV
Comparison between Experimental Interplanar Distances, d_{exptl}, and Calculated Interplanar Distances, d_{calcd}, of PMEPL's for a Monoclinic Crystal Structure[a]

PMEPL-RAC				PMEPL-*S*(−)-27				PMEPL-*S*(−)-74				PMEPL-*S*(−)-99				PMEPL-*R*(+)-97			
d_{exptl}	d_{calcd}	I	*hkl*	d_{exptl}	d_{calcd}	I	*hkl*	d_{exptl}	d_{calcd}	I	*hkl*	d_{exptl}	d_{calcd}	I	*hkl*	d_{exptl}	d_{calcd}	I	*hkl*
0.850	0.847	VS	100	0.848	0.847	VS	100	0.907	0.906	S	100	0.907	0.908	S	100	0.908	0.908	S	100
0.586	0.586	VS	$1\bar{2}0$	0.580	0.579	VS	$1\bar{2}0$	0.566	0.566	VS	$1\bar{2}0$	0.565	0.567	VS	$1\bar{2}0$	0.572	0.572	VS	$1\bar{2}0$
---	---	-	---	---	---	-	---	0.514	0.517	W	011, 020	0.521	0.520	M	011, 020	0.526	0.526	M	011, 020
0.510	0.507	VS	020, $1\bar{1}1$	0.507	0.507	VS	020, $1\bar{1}1$	---	---	-	---	0.495	0.498	M	$1\bar{1}1$, $2\bar{1}0$	0.495	0.499	M	$1\bar{1}1$, $2\bar{1}0$
0.475	0.479	VW	$2\bar{1}0$	---	---	-	---	---	---	-	---	---	---	-	---	---	---	-	---
0.449	0.449	W	200, $2\bar{2}0$	---	---	-	---	0.449	0.452	S	200, $2\bar{2}0$	0.449	0.446	S	200, $2\bar{2}0$	0.451	0.450	S	200, $2\bar{2}0$
0.425	0.424	M	$1\bar{2}1$	---	---	-	---	---	---	-	---	---	---	-	---	---	---	-	---
0.406	0.407	M	021, 111	0.404	0.406	M	021, 111	0.386	0.385	VW	121	---	---	-	---	0.393	0.394	W	121
0.372	0.378	W	$2\bar{1}1$	0.377	0.378	VW	$2\bar{1}1$	0.378	0.382	M	$2\bar{1}1$	0.384	0.386	W	$2\bar{1}1$	0.383	0.386	M	$2\bar{1}1$
---	---	-	---	---	---	-	---	0.361	0.361	W	201, 210	---	---	-	---	0.367	0.364	W	201, 210, $2\bar{2}1$
---	---	-	---	---	---	-	---	0.348	0.345	M	030	---	---	-	---	0.353	0.353	W	030
0.325	0.319	M	121, $3\bar{2}0$	0.321	0.319	M	121, $3\bar{2}0$	---	---	-	---	0.333	0.327	W	121, $3\bar{2}0$	0.330	0.328	M	121, $3\bar{2}0$
---	---	-	---	---	---	-	---	0.318	0.310	VW	211, $2\bar{3}1$	0.313	0.311	VW	211, $2\bar{3}1$	0.312	0.311	VW	211, $2\bar{3}1$
---	---	-	---	---	---	-	---	---	---	-	---	---	---	-	---	0.292	0.289	VW	130, 220
0.292	0.293	VW	012, 102	0.292	0.292	VW	012, 102	---	---	-	---	0.283	0.286	VW	012, 102	0.284	0.285	VW	012, 102
0.269	0.272	VW	220	---	---	-	---	---	---	-	---	---	---	-	---	0.271	0.268	VW	112, 301
0.227	0.229	VW	0.32, 212	0.230	0.229	VW	0.32, 212	0.233	0.228	VW	0.32, 212	0.235	0.229	VW	032, 212	0.237	0.239	VW	032, 212

[a] VS = very strong, S = strong, M = medium, W = weak, and VW = very weak. d_{exptl} and d_{calcd} are given in nm. I = experimental intensity.

Table V
Crystal Structure Characteristics of PMEPL's, Poly(pivalolactone) (PPL), Poly(α-methyl-α-n-propyl-β-propiolactone) (PMPPL), Poly(β-butyrolactone) (PβBL), and Poly(β-valerolactone) (PβVL)

polymer	crystal system	space group	crystal dimensions a/nm	b/nm	c/nm	γ/deg	φ/nm	density/(g/cm³) amorp	cryst	polymer
PMEPL-RAC	monoclinic	$P2_1$-C_2^2	0.96	1.19	0.61	118	0.003	1.07	1.23	1.115
PMEPL-S(−)-27	monoclinic	$P2_1$-C_2^2	0.96	1.17	0.61	118	0.004		1.25	
PMEPL-S(−)-74	monoclinic	$P2_1$-C_2^2	1.00	1.15	0.60	115	0.004		1.21	
PMEPL-S(−)-99	monoclinic	$P2_1$-C_2^2	1.00	1.15	0.60	115	0.003	1.09	1.21	1.134
PMEPL-R(+)-97	monoclinic	$P2_1$-C_2^2	1.00	1.16	0.60	115	0.002		1.20	
PPL[47,48]	monoclinic	$P2_1/b$-C_{2h}^5	0.905	1.158	0.603	121.5	0.0004	1.10	1.234	
PMPPL[43]	monoclinic	$P2_1$-C_2^2	1.10	1.21	0.60	121	0.006	1.05	1.24	1.07
PβBL[53]	orthorhombic	$P2_12_12_1$-D_2^4	0.596	1.320	0.596	90.0			1.26	1.24
PβVL[54]	orthorhombic	$P2_12_12_1$-D_2^4	0.932	1.002	0.556	90.0			1.28	1.20

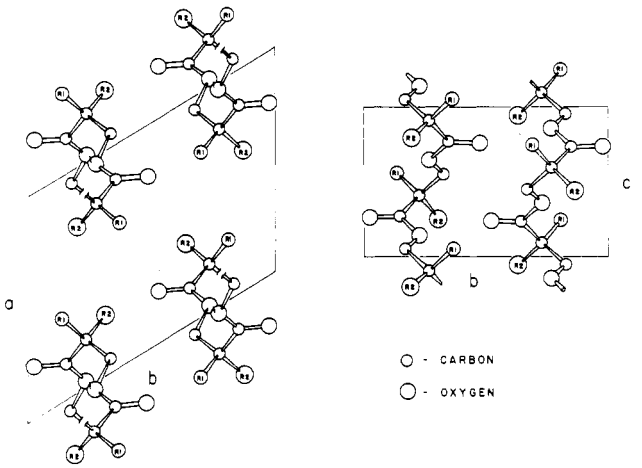

Figure 12. *ab* and *bc* projections of the unit cell of optically pure PMEPL.

conformation, with a periodicity of about 0.6 nm, when the substituents R_1, R_2, and R_3 are not too bulky.[46-52] These substituents are normally pointing away from the helix axis. This sort of conformation is analogous to the α-helical conformation of polypeptides.

The crystalline arrangement of polylactones is only stabilized by interactions between nonbonded atoms since hydrogen bonds are not found in these polymers. Their final conformation depends upon the bulkiness of the substituents. Small fluctuations in the size of the substituents can lead to different crystal structures and unit cell dimensions. For several polylactones, it has been shown in the literature that R_3 is pointing in the same direction as the carbonyl group and in a perpendicular direction to R_1 and R_2.[47,48,50,53,54] As a result of that, α- and β-substituted polylactones are expected to have different crystal structures. In Table V, the β-substituted polylactones are reported to have an orthorhombic crystal structure whereas the α,α-disubstituted polylactones exhibit a monoclinic crystal structure.

Figure 12 shows the *ab* and *bc* projections of the proposed unit cell of optically active PMEPL, where we have assumed a similar crystal structure for PMEPL and PPL and have used the atomic coordinates in the crystalline conformation given in ref 47 and 48. An antiparallel packing of the neighboring chains is required in the *bc* plane. Each chain is then identical with its second neighbor. The methyl groups (R_1) of PMEPL are all oriented in the same direction (in the *bc* projection, they are oriented toward the top of Figure 12) and the ethyl groups (R_2) are oriented in a different direction (toward the bottom of Figure 12 in the *bc* plane). The packing of the chain is then optimized since the R_2 substituents are always facing the R_1 substituents; in other words, bulky substituents are always in front of small substituents. This efficient packing can be reached for stereoregular PMEPL's containing few tacticity defects. It can be reached for PMEPL-S(−)-99 and PMEPL-R(+)-97 and these two polymers have identical crystalline properties.

The racemic polymer unit cell is also made of antiparallel chains. However, it does not have a stereoregular structure, contrary to the optically active polymers, which are isotactic. Consequently, the position of its substituents R_1 and R_2 is random. In the unit cell, all R_1 are not directed in one direction and all R_2 in a different direction. Their direction is determined at random. A bulky R_2 substituent can face another bulky substituent, creating some interference. This interference leads to disorder in the chain packing. This disorder leads to a decrease in $T_f°$ of 43 °C and in ΔH_f of 32 J/g as compared with those of PMEPL-S(−)-99. Schmidt[8] observed a similar behavior for racemic and optically active poly(β-butyrolactams), where the latter has a melting point 17 °C higher than the former. Polylactam crystal structures are stabilized by hydrogen bonds whereas polylactones are not. We therefore expect to observe a greater perturbation in melting point in the former series as compared to the latter due to changes in stereoregularity.

The equilibrium melting points of poly(α,α-disubstituted-β-propiolactones) vary significantly as a function of their substituents. Values of 258, 240, 103, and 121 °C were found for diethyl,[23] dimethyl[21] (PPL), methyl-n-propyl,[11] and methylethyl substituents (racemic polymers only). For symmetric substituents ($R_1 = R_2$), melting points of the order of 247 °C are found. For asymmetric substituents ($R_1 \neq R_2$), the higher the R_1/R_2 ratio, the lower the melting point due to increasing disorder in the chain packing.

Despite the 0.6-nm periodicity found for a large number of polylactones of formula $-[CHR_3CR_1R_2COO]-_n$, indicating a 2_1-helical conformation of the chain, the simplest member of the series, poly(β-propiolactone) (PβL), where $R_1 = R_2 = R_3 = H$, shows a periodicity of 0.702 nm and a low equilibrium melting point at 121 °C.[22,55-57] This exception resembles that met with poly(α-amino acids) where the simplest polypeptide, poly(L-alanine), does not follow the regular α-helical conformation of the other members of the series.[58] PβL does not bear any bulky substituent and it can pack more densely than the substituted poly(β-propiolactones). A more extended helix favors the more efficient packing. PβL has a crystalline density of 1.445 g/cm³,[57] a value that is higher than those found for other substituted poly(β-propiolactones) (Table V).

Measurements presented in this paper finally indicate that the crystalline properties of racemic and optically active PMEPL's are very different: different equilibrium melting points, different enthalpies of fusion, different

melting endotherms, different crystallization rates, and different crystal structures. These differences are due to the stereoregularity of the optically active polymers as compared to the atacticity of the racemic one. However, our measurements indicate at the same time that the amorphous properties of racemic and optically active PMEPL's are very similar: similar interfacial free energies, similar work of chain folding, and similar T_g's. The stereoregularity of the poly(α,α-disubstituted-β-propiolactones) has then a pronounced influence on their crystallization behavior but not on their properties in the melt.

Acknowledgment. We thank Dr. Nicolas Spassky and Alain Leborgne, from the Université Pierre et Marie Curie in Paris, for their collaboration in the synthesis of all PMEPL's used in this work. We also thank the Natural Sciences and Engineering Research Council of Canada and the Ministry of Education of the Province of Québec (FCAC program) for the fellowships (D.G.) and research grants (R.E.P.) that supported this work.

Registry No. *rac*-PMEPL, 84129-15-7; *rac*-PMEPL (repeating unit), 80159-49-5; (*S*)-(−)-PMEPL, 84129-16-8; (*S*)-(−)-PMEPL (repeating unit), 80159-70-2; (*R*)-(+)-PMEPL, 80159-72-4; (*R*)-(+)-PMEPL (repeating unit), 80159-48-4.

References and Notes

(1) Tsuruta, T. *J. Polym. Sci., Part D* **1972**, *6*, 179.
(2) Sigwalt, P. *Pure Appl. Chem.* **1976**, *48*, 257.
(3) Sepulche, N.; Spassky, N.; Sigwalt, P. *Isr. J. Chem.* **1976/1977**, *15*, 33.
(4) Spassky, N. *ACS Symp. Ser.* **1977**, *No. 59*, 191.
(5) Leborgne, A.; Spassky, N.; Sigwalt, P. *Polym. Bull.* **1979**, *1*, 825.
(6) Spassky, N.; Leborgne, A.; Reix, M.; Prud'homme, R. E.; Bigdeli, E.; Lenz, R. W. *Macromolecules* **1978**, *11*, 716.
(7) Grenier, D.; Leborgne, A.; Spassky, N.; Prud'homme, R. E. *J. Polym. Sci., Polym. Phys. Ed.* **1981**, *19*, 33.
(8) Schmidt, E. *Angew. Makromol. Chem.* **1970**, *14*, 185.
(9) D'Hondt, C.; Lenz, R. W. *J. Polym. Sci., Polym. Chem. Ed.* **1978**, *16*, 261.
(10) Carrière, F. J.; Eisenbach, C. D. *Makromol. Chem.* **1981**, *182*, 325.
(11) Grenier, D.; Leborgne, A.; Spassky, N.; Prud'homme, R. E. *J. Polym. Sci., Polym. Chem. Ed.* **1981**, *19*, 1781.
(12) Grenier, D. Ph.D. Thesis, Université Laval, 1982.
(13) Stein, R. S.; Misra, A.; Yuasa, T.; Khambatta, F. *Pure Appl. Chem.* **1977**, *49*, 915.
(14) Pelzbauer, Z.; St. John Manley, R. *J. Polym. Sci., Part A-2* **1970**, *8*, 649.
(15) Lemstra, P. J.; Kooistra, T.; Challa, G. *J. Polym. Sci., Part A-2* **1969**, *10*, 117.
(16) Roberts, R. C. *Polymer* **1969**, *10*, 117.
(17) Roberts, R. C. *J. Polym. Sci., Part B* **1970**, *8*, 381.
(18) Bell, J. P.; Dumbleton, J. H. *J. Polym. Sci., Part A-2* **1969**, *7*, 1033.
(19) Bell, J. P.; Slade, P. E.; Dumbleton, J. H. *J. Polym. Sci., Part A-2* **1969**, *7*, 1033.
(20) Borri, C.; Bruckner, S.; Crescenzi, V.; Della Fortuna, G.; Mariano, A.; Scaragatto, P. *Eur. Polym. J.* **1971**, *7*, 1515.
(21) Prud'homme, R. E.; Marchessault, R. H. *Makromol. Chem.* **1974**, *175*, 2705.
(22) Crescenzi, V.; Manzini, G.; Calzolari, G.; Borri, C. *Eur. Polym. J.* **1972**, *8*, 449.
(23) Normand, Y.; Aubin, M.; Prud'homme, R. E. *Makromol. Chem.* **1979**, *180*, 769.
(24) Ikeda, M. *Kobunshi Kagaku* **1969**, *26*, 102.
(25) Cornibert, J.; Marchessault, R. H.; Allegrezza, A. E.; Lenz, R. W. *Macromolecules* **1973**, *6*, 676.
(26) Hoffman, J. D.; Weeks, J. J. *J. Res. Natl. Bur. Stand., Sect. A* **1962**, *66*, 13.
(27) Flory, P. J. "Principles of Polymer Chemistry"; Cornell Univeristy Press: Ithaca, NY, 1953.
(28) Turnbull, D.; Fisher, J. C. *J. Chem. Phys.* **1949**, *17*, 71.
(29) Hoffman, J. D. *SPE Trans.* **1964**, *4*, 315.
(30) Suzuki, T.; Kovacs, A. J. *Polym. J.* **1970**, *1*, 82.
(31) Williams, M. L.; Landel, R. F.; Ferry, J. D. *J. Am. Chem. Soc.* **1955**, *77*, 3701.
(32) Hoffman, J. D.; Weeks, J. J. *J. Chem. Phys.* **1962**, *37*, 1723.
(33) Magill, J. H. *J. Appl. Phys.* **1964**, *35*, 3249.
(34) Magill, J. H. *J. Polym. Sci., Part A-2* **1967**, *5*, 89.
(35) Magill, J. H. *J. Polym. Sci., Part A-2* **1969**, *7*, 1187.
(36) Pollack, S. S.; Magill, J. H. *J. Polym. Sci., Part A-2* **1969**, *7*, 551.
(37) Godovsky, Y. K.; Slonimsky, G. L. *J. Polym. Sci., Polym. Phys. Ed.* **1974**, *12*, 1053.
(38) Hoffman, J. D.; Frolen, L. J.; Ross, G. S.; Lauritzen, J. I. *J. Res. Natl. Bur. Stand., Sect. A* **1975**, *79*, 671.
(39) Lauritzen, J. I. *J. Appl. Phys.* **1973**, *44*, 4353.
(40) Hoffman, J. D.; Weeks, J. J. *J. Chem. Phys.* **1962**, *37*, 1723.
(41) Lauritzen, J. I.; Hoffman, J. D. *J. Res. Natl. Bur. Stand., Sect. A* **1960**, *64*, 73.
(42) Noah, J.; Prud'homme, R. E. *Macromolecules* **1979**, *12*, 300.
(43) Grenier, D. M.Sc. Thesis, Laval University, 1979.
(44) Prud'homme, R. E.; Stein, R. S. *J. Polym. Sci., Polym. Phys. Ed.* **1973**, *11*, 1357.
(45) Stein, R. S.; Rhodes, M. B. *J. Appl. Phys.* **1960**, *31*, 1873.
(46) Duchesne, D.; Prud'homme, R. E. *Polymer* **1979**, *20*, 1199.
(47) Carrazzolo, G. *Chim. Ind. (Milan)* **1964**, *46*, 525.
(48) Perego, G.; Malis, A.; Cesari, M. *Makromol. Chem.* **1972**, *157*, 269.
(49) Prud'homme, R. E.; Marchessault, R. H. *Macromolecules* **1974**, *7*, 541.
(50) Cornibert, J.; Hien, N. V.; Brisse, F.; Marchessault, R. H. *Can. J. Chem.* **1974**, *52*, 3742.
(51) Cornibert, J.; Marchessault, R. H.; Allegrezza, A. E.; Lenz, R. W. *Macromolecules* **1973**, *6*, 676.
(52) Marchessault, R. H.; St Pierre, J.; Duval, M.; Perez, S. *Macromolecules* **1978**, *11*, 1281.
(53) Yokouchi, M.; Chatani, Y.; Tadokoro, H.; Teranishi, K.; Tani, H. *Polymer* **1973**, *14*, 267.
(54) Yokouchi, M.; Chatani, Y.; Tadokoro, H.; Tani, H. *Polym. J.* **1974**, *6*, 248.
(55) Wasai, K.; Saegusa, T.; Furukawa, J. *Kogyo Kagaku Zasshi* **1964**, *67*, 601.
(56) Kagiga, T.; Sano, T.; Fukui, K. *Kogyo Kagaku Zasshi* **1964**, *67*, 451.
(57) Suehiro, K.; Chatani, Y.; Tadokoro, H. *Polym. J.* **1975**, *7*, 352.
(58) Bamford, C. H.; Elliot, A.; Hanby, W. E. "Synthetic Polypeptides"; Academic Press: New York, 1956.
(59) Price, F. P. *J. Am. Chem. Soc.* **1952**, *74*, 311.